ACS APPLIED ENERGY MATERIALS

www.acsaem.org Article

Light Induced Ion Migration Studies in Perovskite Solar Cell Using Nonlinear Impedance Spectroscopy

Sanish Paramadam, Benjamin W. Howe, Seid Yimer Abate, Randall Headrick, and Matthew S. White*

Cite This: https://doi.org/10.1021/acsaem.5c00672 Read Online

ACCESS | Metrics & More | Article Recommendations | Supporting Information

ABSTRACT: Complex interactions between mobile ions and charge carriers in perovskite solar cells (PSCs) make it challenging to fully understand their dynamic interplay. Exposure to light further complicates these interactions, altering the system's dynamics and inducing nonlinear effects that lead to changes in the $J-V$ curve. Understanding these effects is crucial for improving the operational stability of PSCs. Impedance spectroscopy (IS) is a powerful technique for evaluating relaxation processes in the frequency domain; however, it is limited in capturing nonlinear contributions. In this work, nonlinear impedance spectroscopy (NLIS) is employed to analyze the higher harmonic response to AC perturbation, both in the dark and after short-term light exposure. A shift in the low-frequency (LF) higher harmonic peak is observed after open-circuit light exposure, attributed to an altered electric field suggesting ion redistribution, whereas closed-circuit exposure shows no LF shift, indicating minimal ion movement. Additionally, light exposure reduces higher-order admittance, more notably in open-circuit conditions, suggesting decreased recombination. Temperature-dependent analysis was conducted to characterize the activation energy of migrating species, identifying iodide as the dominant migrating ion.

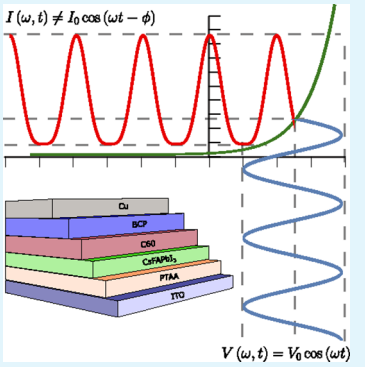

KEYWORDS: *perovskite solar cells, nonlinear impedance spectroscopy, higher-order admittance, light-induced ion migration, ionic-electronic coupling, open-circuit light exposure*

INTRODUCTION

Organic−inorganic hybrid perovskite solar cells offer promising advantages compared to conventional photovoltaic technologies, including the ease of fabrication,[1] potentially low cost of fabrication,[2] high power conversion efficiencies[3] and band gap tunability.[4] Perovskites are used as the active, light-absorbing layer in solar cells and consist of a structure denoted as ABX_3, where A represents an organic or inorganic monovalent cation, such as cesium (Cs^+), methylammonium (MA^+), or formamidinium (FA^+); B is a divalent metal, such as Pb^{2+} or Sn^{2+}; and X is a halide, such as I^-, Br^-, or Cl^-. The presence of ions in the perovskite structure enables bandgap tunability, which is one of the most significant benefits of perovskite solar cells(PSC) among new-generation PV technologies.[4] Thus,perovskites offer a range of tunable parameters for tailoring optical and electronic properties, making them promising candidates for optoelectronic applications, including solar cells.[5] The certified record cell efficiency for perovskite PV has grown from 9.7%[6] in 2012 to 27%[7] in 2025. However, the same variables that enable the tuning of functional properties, such as bandgap tunability in perovskites, also introduce significant variability in the operational and degradation mechanisms of these materials and devices. Exposure to heat and light activates mobile ionic defects,[8,9] which can migrate and deform the structure, contributing to the overall degradation of PSCs and significantly impacting their long-term operational stability.[10]

Mobile ions generated due to light exposure also lead to changes in the dark $J-V$ curve, a phenomenon commonly observed in PSCs.[11] Therefore, understanding these processes is crucial for addressing challenges related to stability.

Impedance spectroscopy (IS) is a powerful, frequency-domain technique used to analyze these effects. IS involves applying a small AC voltage, with or without an applied DC bias, across a wide range of frequencies and measuring the amplitude and phase of the resulting current, with impedance (Z) defined as the ratio of voltage to current.

$$V(\omega, t) = V_0 \cos(\omega t) \tag{1}$$

$$I(\omega, t) = I_0 \cos(\omega t - \Phi) \tag{2}$$

$$Z(\omega, t) = \frac{V_0 \cos(\omega t)}{I_0 \cos(\omega t - \Phi)} \tag{3}$$

Where V_0 and I_0 are input voltage and current respectively and ω is the frequency, ϕ is relative phase difference.

Received: March 6, 2025
Revised: June 7, 2025
Accepted: June 10, 2025

IS data for perovskite solar cells tends to show different relaxation processes at their characteristic frequencies.[12] High frequency(HF) features can be attributed to geometric capacitance and bulk recombination,[13] while Low frequency-(LF) attributes are associated with slower ionic process.[14] IS methods have limitations, as they treat the system as linear and time-independent. Additionally, IS methods rely on equivalent circuit models[15] for analysis, but these models often include passive circuits and constant phase elements that may lack substantial physical meaning. This is especially true for PSCs, which are diodes and inherently exhibit a nonlinear electronic response. Moreover, processes like hysteresis, resulting from mobile ions, are purely nonlinear in nature. Therefore, the assumption of linearity is insufficient to fully understand the system. Measurement of the nonlinear response in the frequency domain can provide valuable insights into these mechanisms. Thus, we employ the method of nonlinear impedance spectroscopy (NLIS). The NLIS technique employs slightly higher amplitude AC signal perturbation for analysis and characterizes the output signal using Fourier transform (FT). The NLIS characterization technique has previously been used in the analysis of p-n junction diode,[16] organic heterojunctions, MIS capacitors,[17] fuel cells,[18] lithium-ion batteries,[19] and thermoelectric materials.[20] To the best of our knowledge, NLIS as a characterization technique has not been previously applied to PSCs.

NLIS applies an AC voltage as in eq 1 but the resultant current is not sinusoidal due to the nonlinear response, and therefore

$$I(\omega, t) \neq I_0 \cos(\omega t - \Phi) \tag{4}$$

The obtained periodic signal can be expanded using Fourier expansion

$$I(\omega, t) = a_0 + \sum_{n=1}^{\infty} A_n \cos(n\omega t + \phi_n) \tag{5}$$

$$A_n = \frac{2}{T\cos(\phi_n)} \int_0^T I(\omega, t)\cos(n\omega t)\mathrm{d}t \tag{6}$$

ω is the fundamental frequency of the input wave. The frequency analyzer used in experiment measures the Fourier coefficients (A_n) directly for all frequencies and ϕ_n for frequencies lower than 1500 Hz if $n > 1$.) The measured A_n serve as a basis for calculating properties relevant to the device and the component materials.[16,17] In the low frequency limit, the measured current waveform could be expressed as the Taylor series expansion about the point (V_{DC}, I_{DC}):

$$I(\omega, t) = I_{DC} + \sum_{n=1}^{\infty} \left.\frac{\mathrm{d}^n I}{\mathrm{d}V^n}\right|_{V_{DC}} (V(\omega, t))^n \tag{7}$$

By combining the expressions in eqs 5 and 7, the Fourier coefficients A_n can be expressed in terms of the derivatives of the functional relation between current and voltage. These Fourier coefficients take slightly different forms for the even and odd terms:

$$A_{2n} = \sum_{m=n}^{\infty} \frac{1}{2^{2m}(m-n)!(m+n)!} \left.\frac{\mathrm{d}^{2m} I}{\mathrm{d}V^{2m}}\right|_{V_{DC}} V_0^{2m} \tag{8}$$

$$A_{2n+1} = \sum_{m=n}^{\infty} \frac{1}{2^{2m}(m-n)!(m+n+1)!} \left.\frac{\mathrm{d}^{2m+1} I}{\mathrm{d}V^{2m+1}}\right|_{V_{DC}} V_0^{2m+1} \tag{9}$$

These derivatives of current with respect to voltage are analogous to the definition of admittance Y and impedance Z,

$$Y = \frac{1}{Z}, \lim_{\omega \to 0} Y_n(\omega) = \frac{\mathrm{d}^n I}{\mathrm{d}V^n} \tag{10}$$

By substituting Y_n in place of $\frac{\mathrm{d}^n I}{\mathrm{d}V^n}$ in eqs 8 and 9 and extending throughout the frequency domain, we can define $Y_n(\omega)$ in terms of the measured $A_n(\omega)$.

If the current−voltage relationship is entirely linear, all higher-order derivatives beyond $\frac{\mathrm{d}I}{\mathrm{d}V}$ are zero, allowing conventional impedance spectroscopy to fully describe the system's behavior. However, in PSCs, where nonlinearity is inherent, higher-order derivatives produce non-negligible measurable higher harmonic signals (A_m). Furthermore, if a system exhibits a measurable nonlinear response at order m, then this will perturb the measurements of all lower order signals A_n with $n < m$ provided that both n and m share the same parity (even or odd). For example, space charge limited current exhibits a quadratic relationship between voltage and current, and yields A_1 and A_2, but no higher order coefficients.[17] The presence of the nonzero A_2 does not influence the fundamental admittance Y_1. However, in the case of exponential recombination current, there are infinite even and odd coefficients of progressively smaller magnitude, and Y_1 is defined in terms of all measurable odd A_n above the noise threshold. Analyzing the higher harmonics over the frequency domain enables the direct characterization of underlying nonlinear processes and their relation to different physical mechanisms in PSCs. In this study, nonlinear impedance spectroscopy (NLIS) is applied for the first time to PSCs to investigate the effects caused by short-term light exposure.

EXPERIMENTAL DETAILS

Materials and Device Fabrication. Lead iodide (PbI_2) was obtained from TCI. Formamidinium iodide (FAI) was sourced from Greatcell Solar Materials. Cesium iodide (CsI), methylammonium chloride (MACl), Buckminsterfullerene (C_{60}), and bathocuproine (BCP) were acquired from Sigma-Aldrich. Poly(triarylamine), specifically Poly[bis(4-phenyl)(2,4,6-trimethylphenyl)amine] (PTAA), was purchased from Ossila. The copper bar was obtained from R.D. Mathis Company. Solvents including *N*,*N*-dimethylformamide (DMF), isopropanol, acetonitrile, ethanol, 2-methoxyethanol, chlorobenzene, dimethyl sulfoxide (DMSO), and gamma-butyrolactone were also purchased from Sigma-Aldrich. All chemicals were used as received, without further purification.

A p-i-n structured device with the architecture ITO/PTAA/CsFAPI/C_{60}/BCP/Cu was fabricated. Initially, a patterned indium tin oxide (ITO) substrate (~20 Ω/sq) was sequentially cleaned with detergent, deionized water, acetone, and isopropanol for 10 min each. The substrate was then dried using an air gun and stored in an oven.

The hole transport material PTAA was dissolved in chlorobenzene at a concentration of 2 mg/mL and spin-coated at 500 rpm for 5 s, followed by 3000 rpm for 30 s, and then annealed at 100 °C for 10 min. The PTAA thin film was subsequently treated with DMF to reduce its hydrophobicity by spin-coating DMF onto the PTAA film at 3000 rpm for 30 s.

The perovskite precursor solution, composed of 1.67 M $Cs_xFA_{1-x}PbI_3$ (where PbI_2:FAI is in a 1:1 molar ratio) with methylammonium chloride (MACl) as an additive, was coated using a Verde slot-die coater and then annealed at 150 °C.

https://doi.org/10.1021/acsaem.5c00672
ACS Appl. Energy Mater. XXXX, XXX, XXX−XXX

Subsequently, C_{60} (26 nm), BCP (8 nm), and Cu (100 nm) were deposited using a thermal evaporator. The device architecture of the PSC is shown in the inset of Figure 1. The PSC consists of Cu (100 nm), BCP (8 nm), C_{60} (26 nm), a perovskite layer (500 nm), PTAA (55 nm), and ITO (100 nm). The PSC was encapsulated using glass and epoxy resin.

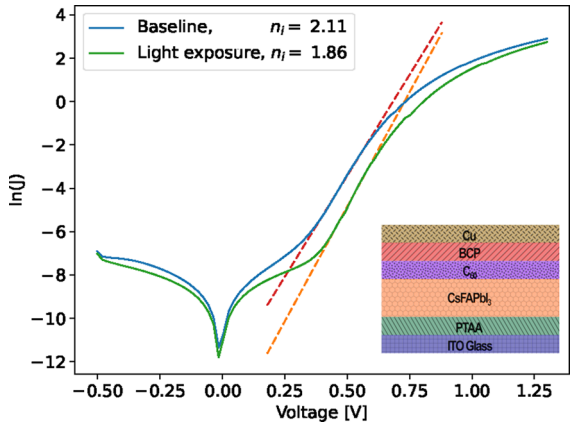

Figure 1. Current density (J)−voltage (V) curve of PSC before and after light exposure.

Device Characterization. The performance of the perovskite solar cells was assessed using a Keithley 2400 digital source meter under approximately 100 mW/cm^2 (1 sun intensity) with a SM2F32-A Thorlabs white LED. Light intensity was calibrated using a standard silicon photodiode, and the active area of the device was 0.15 cm^2. nonlinear impedance analysis was conducted using a Novocontrol Alpha-AT frequency response analyzer connected to the cryogenic workstation under a vacuum of 10^{-5} Torr, as the sample was measured inside the workstation. For low-temperature analysis, liquid nitrogen was supplied through a Dewar to the workstation. A Lakeshore 336 temperature controller was connected to the workstation to precisely control the temperature.

RESULTS AND DISCUSSION

Linear Impedance Spectroscopy. First, to demonstrate the effects of light exposure in PSCs, $J-V$ characterization was performed. Figure 1 shows the $J-V$ curve of the device under dark conditions and immediately after exposure to white light at 1 sun intensity for approximately 15 s, followed by measurement in the dark, both recorded in the forward scan. The light $J-V$ curve is provided in the Supporting Information as Figure S1. Hereafter, the term "after light exposure" refers to characterization performed in the dark following prior light exposure. The diode turn-on voltage for both conditions is observed around 0.35 V, where the current is exponentially proportional to the voltage (recombination-limited regime). Further increases in voltage result in current limited by the series resistance. There is a noticeable difference between the $J-V$ curves measured before and after light exposure. Short-term light exposure causes a shift in the dark current response, as shown in Figure 1. The reduction in dark current after light exposure may indicate a decrease in trap states, a commonly observed effect in perovskite solar cells.[11] The ideality factor obtained from the two conditions, shown in the inset box in Figure 1, supports this observation. The corresponding increase in shunt resistance further reinforces this, with the calculated shunt and series resistance values provided in Table S1. Conventional impedance spectroscopy measures the real and imaginary components of Z, as defined in eq 3, in response to a small AC voltage (50 mV_{rms}). Figure 2a,b shows the real and imaginary parts of the impedance for the PSC. Here, all impedance measurements are conducted under dark conditions. The solid line represents the spectra of the solar cell before light exposure, while the dashed line shows the spectra after light exposure. There are no significant differences between the two spectra. However, when comparing different biases in Figure 2a, as expected, there is an decrease increase in real impedance at low frequencies with increased forward bias, which is a typical characteristic of a diode.

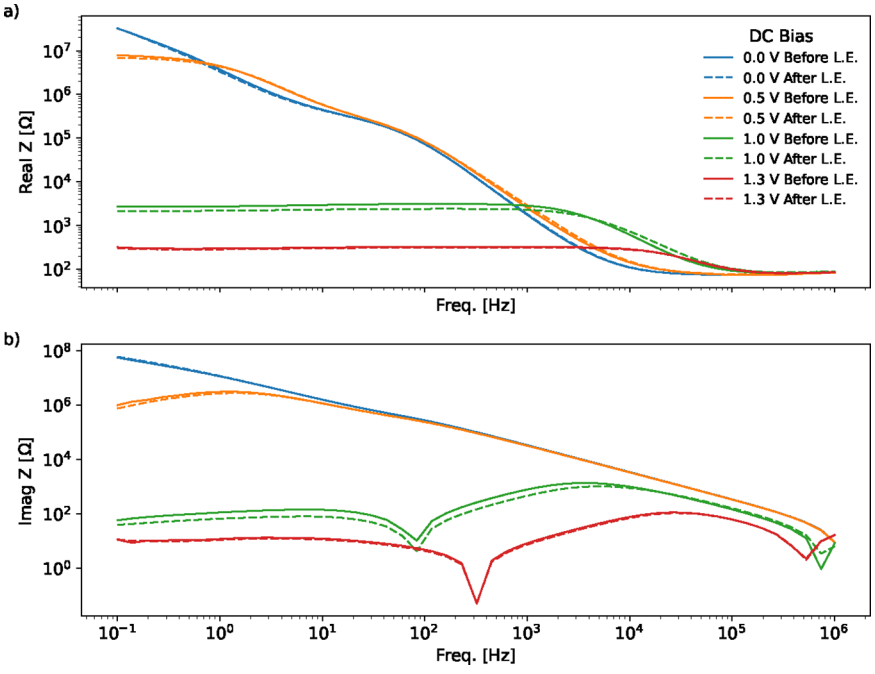

Figure 2. Magnitude of (a) real and (b) imaginary impedance spectra for PSC under various forward DC biases.

https://doi.org/10.1021/acsaem.5c00672
ACS Appl. Energy Mater. XXXX, XXX, XXX−XXX

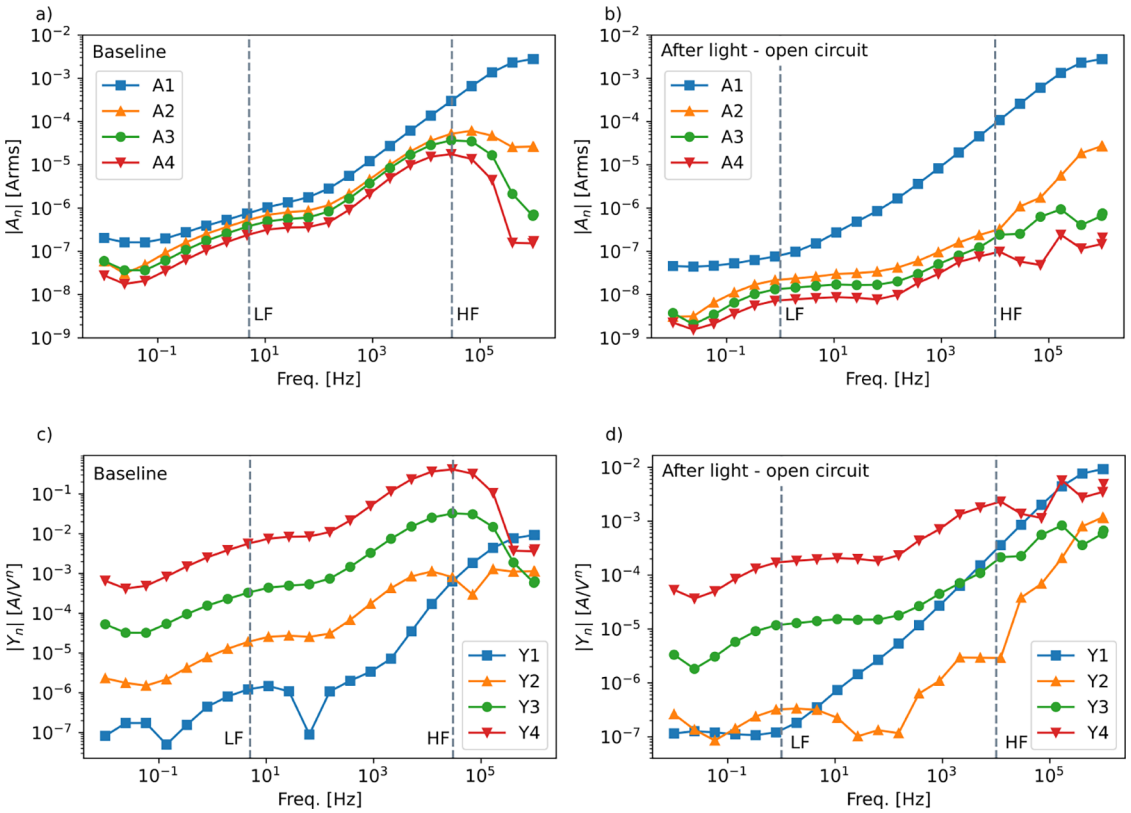

Figure 3. NLIS of the PSC under 0 V bias and 300 mV_{rms} AC amplitude. (a) and (b) show the measured Fourier coefficients A_n of PSC before and after light exposure, respectively. (c) and (d) show the calculated admittance Y_n of PSC before and after light exposure respectively.

Figure 2b shows the absolute imaginary component of Z. The sign of $\mathrm{Im}(Z)$ is negative due to the capacitive behavior of the device. An asymptotic trend in the log−log plot of $\mathrm{Im}(Z)$ vs frequency can be observed for devices biased above 1 V DC. In these cases, $\mathrm{Im}(Z)$ approaches zero and eventually becomes positive. These inductive loops are often referred to as negative capacitance in the linear analysis of the system, a topic of ongoing debate within the community.[21−24] This voltage-dependent negative capacitance is linked to complex nonlinear processes. The influence of nonlinear phenomena in standard impedance spectroscopy arises from the $n = 0$, $m = 1$ term of eq 9. By incorporating the first nonlinear correction, the observed A_1 becomes

$$A_1 = Y_1 V_0 + \frac{Y_3 V_0^3}{8} + \cdots \tag{11}$$

In impedance spectroscopy, these nonlinear correction factors are small because the applied V_0 is small; however, Y_3 might be several orders of magnitude higher than Y_1, which cannot be neglected. Overall, this impedance spectroscopy analysis reveals the presence of nonlinearity in the system, but lacks in providing more details about the nonlinear process. Therefore, we will focus our discussion on NLIS spectra of PSC obtained by applying a slightly higher AC perturbation.

NLIS of PSC. As mentioned above, conventional impedance spectroscopy lacks the ability to provide information on the nature of nonlinear processes in perovskite solar cells. Therefore, we extracted the nonlinear terms using an impedance analyzer and analyzed the first four Fourier coefficients. We employed a 300 mV_{rms} perturbation, as this moderate voltage drives the system beyond the linear regime while not being so high as to reach the series resistance-dominated region. In principle, A_n can be evaluated for any harmonic order, limited only by the signal-to-noise ratio. As the harmonic order increases, the magnitude of the coefficients decreases, making higher-order terms more difficult to resolve. In this study, we chose $n \leq 4$ as it provided sufficient nonlinear signal amplitude while maintaining measurement reliability and experimental practicality. We kept the DC voltage at 0 V to study the nonlinear effects under low carrier injection. All NLIS measurements discussed in this article were conducted in dark conditions. The measured Fourier coefficients from $n = 1$ to $n = 4$ of the PSC are shown as the baseline in Figure 3a. The NLIS spectra of perovskite solar cells (PSC) are plotted as a function of frequency from 10^{-2} Hz to 1 MHz. The spectra clearly show that all four coefficients are well above the detection limit, indicating the strong nonlinear nature of the system. Close monitoring of the nonlinear coefficients A_2, A_3, and A_4 reveals two peaks: one within the LF range of 0.01 to 100 Hz, and another in the HF range of 10^3 to 10^6 Hz.

The higher-order admittance Y_n can be calculated using the A_n signal up to the fourth harmonic, as derived from eqs 8−10, which is not achievable with linear impedance spectroscopy. Higher order admittance Y_2, Y_3, Y_4 enables detailed analysis of nonlinear processes over a wide frequency range. Figure 3c shows the admittance as a function of frequency for the PSC before light exposure. The LF peak indicates slow relaxation process,likely due to ionic relaxation. The HF peak is likely to be associated with fast dynamics, such as rapid electronic processes. After exposure to 1 sun intensity light in open circuit for approximately 15 s, measuring NLIS in the dark yields the results shown in 3b. It is clear that there is a difference in the Fourier coefficients before and after light exposure. The

https://doi.org/10.1021/acsaem.5c00672
ACS Appl. Energy Mater. XXXX, XXX, XXX−XXX

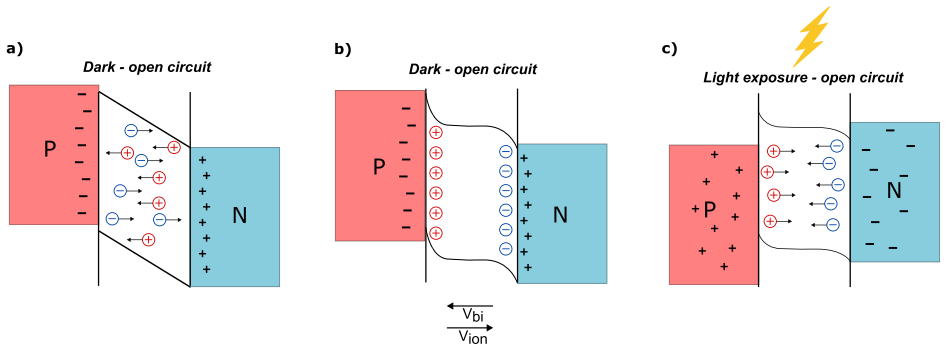

Figure 4. Energy level diagram of PSC (a) right after device fabrication, (b) after attaining equilibrium, (c) right after short-term light exposure in open circuit.

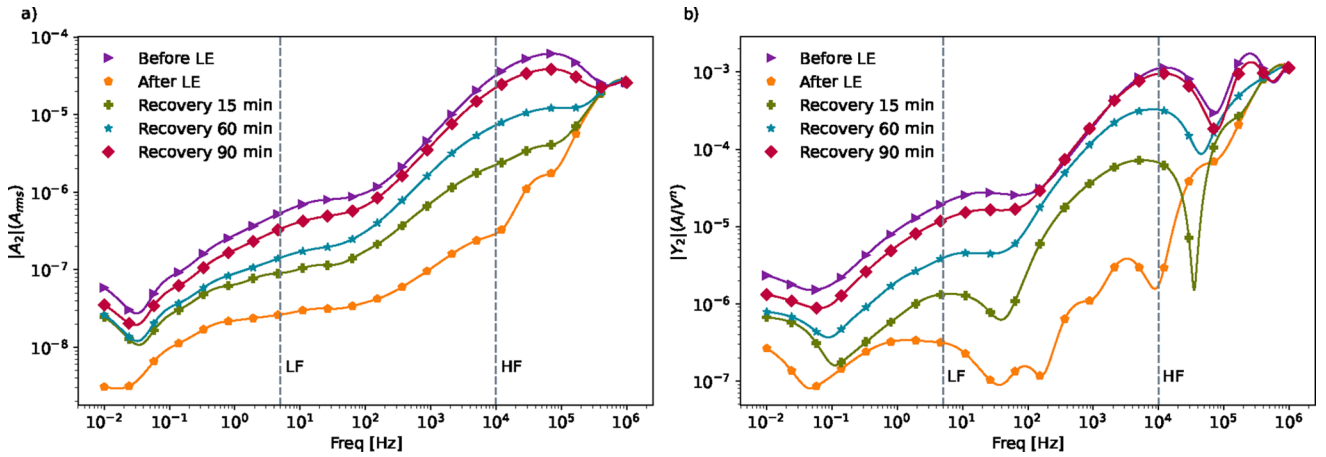

Figure 5. (a) Comparison of Fourier coefficient A_2 of PSC from before light exposure to different recovery times. (b) Comparison of admittance Y_2 of PSC before light exposure to different time of recovery.

Fourier coefficients have shifted down by an order of magnitude after the light exposure. The lower-frequency peaks observed in A_2, A_3, and A_4 in the NLIS spectra before light exposure shift to the left after illumination, indicating possible ionic redistribution. The corresponding admittance Y_n is extracted from the A_n coefficients and plotted against frequency, as shown in Figure 3d. The magnitude of the higher-order admittances Y_2, Y_3, and Y_4 has decreases by an order of magnitude upon light exposure, indicating a reduction in recombination. After light exposure, the LF peak of higher-order admittance shifts to a lower frequency, indicating a change in the time scale. The behavior of Y_1 is characteristic of an RC network, exhibiting a smooth transition from resistive dominance to capacitive dominance across the frequency spectrum. The NLIS data suggest a coupled electronic and ionic process occurring within the perovskite layer. A schematic representation of this process is shown in Figure 4a–c. Ebadi et al. have shown a similar ionic and electronic coupled process in perovskite solar cells.[25] The type and charge of ions/defects depicted in the figures are not related to any specific ion; they are general representations. Figure 4a shows the equilibrium condition where the Fermi levels of the hole transport layer (HTL), perovskite layer, and electron transport layer (ETL) are aligned, generating an internal electric field inside the perovskite layer. Cationic and/or anionic species drift along this electric field, resulting in ion accumulation or depletion at the ETL/perovskite interface and HTL/perovskite interface (Figure 4b). Upon the incidence of white light for a short period at open circuit, the ETL and HTL become charged with electrons and holes respectively, Since the circuit is open, these photogenerated carriers cannot be extracted, resulting in a change in the direction of the internal electric field. This change causes a redistribution of ions, driving anionic species toward the HTL and cationic species toward the ETL (Figure 4c). Thus, the higher values of higher-order admittance before light exposure can result from band bending near the interface due to ion accumulation, which reduces the injection barrier and facilitates the injection of electrons from the ETL and holes from the HTL into the bulk. After light exposure, ion redistribution flattens the band bending (Figure 4c), potentially hindering efficient carrier injection into the bulk and leading to a reduction in higher-order admittance components (Y_2, Y_3, Y_4). The shift of the LF peak in higher-harmonic admittance to the left further supports ionic redistribution from the interface. The evolution of Y_1 after light exposure clearly indicates that the device behaves more linearly.

Light Exposure Recovery. To further assess the reversibility of the effects caused by open circuit light exposure, we measured the NLIS of the device at various intervals after the light exposure. Figure 5a,b shows a comparison of the nonlinear Fourier coefficient A_2 and the nonlinear admittance Y_2 from the baseline (before light exposure), immediately after exposure, and at various recovery times up to 90 min, respectively. Here, one can observe the evolution of the LF peaks in the spectra, gradually shifting back to positions on the frequency scale similar to the baseline (i.e., before light exposure). Compared to the rapid change upon illumination,

https://doi.org/10.1021/acsaem.5c00672
ACS Appl. Energy Mater. XXXX, XXX, XXX−XXX

the slow return of the peak to its baseline position while the solar cell is kept in the dark supports the previously reported observation that light reduces the ion activation energy in perovskites.[26] After the prolonged recovery time, ions reaccumulate at the interfaces, leading to band bending that facilitates electrical injection into the bulk. Overall, the Y_n spectra returning to their pre-exposure baseline supports the reversibility of the effects caused by open-circuit light exposure.

Activation Energy. We further investigated the activation energy of the migrating species by plotting the Arrhenius plot shown in Figure 6, which plots the logarithm of the rate constant against $1/k_BT$. The Arrhenius equations (eqs S1 and S2) are provided in the Supporting Information. The rate constant is obtained from the temperature-dependent Bode plot (imaginary impedance vs frequency), which can be found in the Supporting Information as Figure S2. We obtained a value of 0.43 eV for the activation energy of the migrating species. The plot containing the fit parameters of the Arrhenius analysis is provided in the Supporting Information as Figure S3. Other studies show that the activation energy for iodide ions in similar formamide-based perovskite structures has been found to be in the range of 0.3 to 0.5 eV.[27,28] While cation species can also exhibit similar activation energies, previous studies indicate that the time scale of such processes lies outside the experimental window.[10] Thus, we suspect that the LF response is most likely due to iodide ions. Activation energy measured from low-frequency signals is also highly dependent on the composition of the perovskite,[29−31] and both cationic and anionic substitutions can modify this activation energy.[32]

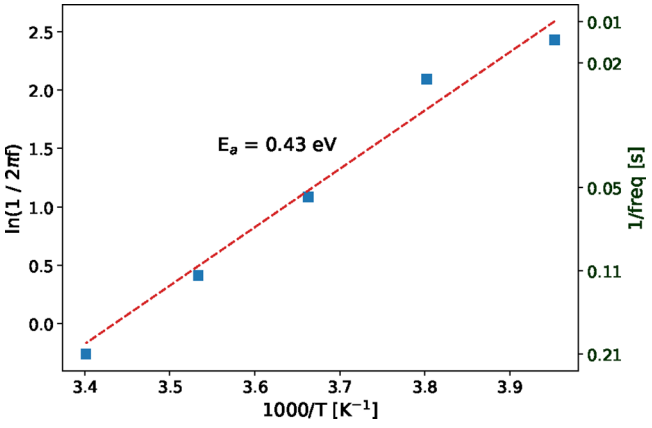

Figure 6. Arrhenius plot of temperature dependence of low-frequency peak.

Effect of Closed Circuit. To reaffirm the hypothesis of ionic displacement due to changes in the internal electric field caused by light exposure under open-circuit conditions, we conducted the same experiment under closed-circuit conditions. The closed-circuit configuration is expected to suppress the buildup of photogenerated charge at the ETL and HTL interfaces, thereby minimizing changes in the internal electric field and reducing ion redistribution upon light exposure. The NLIS spectra after 1.5 h of recovery were taken as the new baseline, as shown in Figure 7a. The calculated admittance (Y_n) is presented in Figure 7b. Both spectra are comparable to the original baseline NLIS spectra

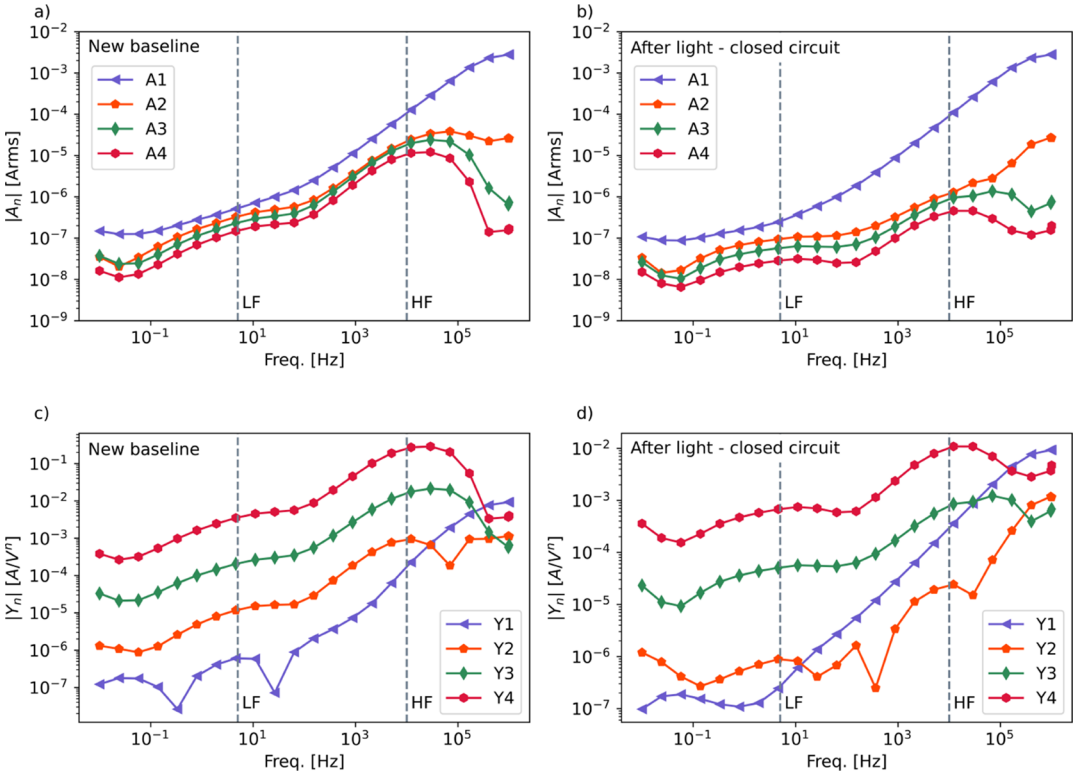

Figure 7. NLIS of the PSC under 0 V bias and 300 mV_{rms} AC amplitude. (a) and (b) show the measured Fourier coefficients A_n of PSC of new baseline and following light exposure at closed-circuit, respectively. (c) and (d) show the calculated admittance Y_n of new baseline and following light exposure at closed-circuit, respectively.

https://doi.org/10.1021/acsaem.5c00672
ACS Appl. Energy Mater. XXXX, XXX, XXX−XXX

shown in Figure 3a,c, respectively. The measured Fourier coefficient (A_n) and the calculated admittance (Y_n) after the closed-circuit light exposure are shown in Figure 7b,d, respectively. Analyzing both (A_n) and (Y_n) after light exposure under closed-circuit conditions, no change in the position of the LF peaks is observed, indicating minimal ion displacement.

Since the circuit is closed during light exposure, photoinduced electrons and holes injected into the ETL and HTL, respectively, flow freely through the external circuit. This prevents the accumulation of photogenerated charge carriers at the ETL and HTL, resulting in minimal changes to band bending, unlike under open-circuit conditions (see Figure 3d). This results in minimizing the ion redistribution. Interestingly, a decrease in the magnitude of higher-order admittance can be observed after closed-circuit light exposure, though it is not as pronounced as in the open-circuit condition. The increased magnitude of Y_1 compared to Y_2 (for frequencies >10 Hz) follows a similar trend to the admittance spectra observed after open-circuit light exposure (Figure 3d), suggesting that light exposure, whether under closed- or open-circuit conditions, influences the device behavior. This is in agreement with previously observed phenomena in photoluminescence microscopy characterization of perovskite solar cells showing that short-term light exposure in both open- and closed-circuit conditions reduces nonradiative recombination, with the effect being more pronounced in the open-circuit condition.[33]

CONCLUSIONS

We investigated the higher harmonic response to AC perturbation in perovskite solar cells using Fourier analysis. Higher harmonic Fourier coefficients help filter out linear processes, as purely capacitive and resistive processes do not contribute to A_n for $n > 1$. Evaluating these coefficients across various frequency ranges enables the calculation of higher-order admittance, facilitating the direct characterization of nonlinear processes in PSCs. The presence of relaxation peaks in the higher harmonic response at distinct frequency ranges differentiates electronic and ionic relaxation. Short-term open-circuit light exposure shifts the low-frequency peak to a lower frequency, suggesting ionic redistribution due to carrier accumulation in the ETL and HTL. In contrast, under closed-circuit conditions, carrier accumulation is suppressed, preventing ion redistribution to the same degree, as confirmed by the absence of a low-frequency peak shift. Additionally, light exposure in both open- and closed-circuit conditions results in a reduction in higher-order admittance, indicating decreased recombination. Temperature-dependent analysis enables the characterization of the activation energy of migrating species and aids in their identification. Nonlinear impedance spectroscopy allows for the characterization of dynamic processes from MHz to mHz frequency scales, similar to conventional impedance spectroscopy, while distinguishing contributions to the response from recombination, injection and transport processes. It enabled the direct characterization of changes in nonlinear dynamics resulting from short-term light exposure in perovskite solar cells.

ASSOCIATED CONTENT

Supporting Information

The Supporting Information is available free of charge at https://pubs.acs.org/doi/10.1021/acsaem.5c00672.

Light $J-V$ curve of the PSC, temperature-dependent Cole plot of PSC, Arrhenius equation, and activation energy fit parameters (PDF)

AUTHOR INFORMATION

Corresponding Author

Matthew S. White − *Materials Science Program and Department of Physics, University of Vermont, Burlington, Vermont 05405, United States;* orcid.org/0000-0001-6719-790X; Email: matthew25@uvm.edu

Authors

Sanish Paramadam − *Materials Science Program, University of Vermont, Burlington, Vermont 05405, United States*

Benjamin W. Howe − *Department of Physics and Materials Science Program, University of Vermont, Burlington, Vermont 05405, United States*

Seid Yimer Abate − *Department of Physics and Materials Science Program, University of Vermont, Burlington, Vermont 05405, United States*

Randall Headrick − *Department of Physics and Materials Science Program, University of Vermont, Burlington, Vermont 05405, United States*

Complete contact information is available at: https://pubs.acs.org/10.1021/acsaem.5c00672

Notes

The authors declare the following competing financial interest(s): Randall L. Headrick is founder and Head of Science of Verde Technologies, a company commercializing perovskite photovoltaics. A family member of Matthew S. White is employed by VEIC, an energy consulting company with supporting role in the DOE EERE award DE-EE0010147.

ACKNOWLEDGMENTS

This material is based upon work supported by the U.S. Department of Energy's Office of Energy Efficiency and Renewable Energy (EERE) under the Solar Energy Technologies Office Award Number DE-EE0010147. The views expressed herein do not necessarily represent the views of the U.S.Department of Energy or the United States Government.The work at UVM is supported by DOE grant DE-EE0010147, USA. S.A. acknowledges support from Verde Technologies Inc.

REFERENCES

(1) Correa-Baena, J.-P.; Saliba, M.; Buonassisi, T.; Grätzel, M.; Abate, A.; Tress, W.; Hagfeldt, A. Promises and challenges of perovskite solar cells. *Science* **2017**, *358*, 739−744.

(2) Snaith, H. J. Perovskites: The Emergence of a New Era for Low-Cost, High-Efficiency Solar Cells. *J. Phys. Chem. Lett.* **2013**, *4*, 3623−3630.

(3) Zhou, J.; Tan, L.; Liu, Y.; Li, H.; Liu, X.; Li, M.; Wang, S.; Zhang, Y.; Jiang, C.; Hua, R.; Tress, W.; Meloni, S.; Yi, C. Highly efficient and stable perovskite solar cells via a multifunctional hole transporting material. *Joule* **2024**, *8*, 1691−1706.

(4) Eperon, G. E.; Stranks, S. D.; Menelaou, C.; Johnston, M. B.; Herz, L. M.; Snaith, H. J. Formamidinium lead trihalide: a broadly tunable perovskite for efficient planar heterojunction solar cells. *Energy Environ. Sci.* **2014**, *7*, 982−988.

(5) Chen, Q.; De Marco, N.; Yang, Y. M.; Song, T.-B.; Chen, C.-C.; Zhao, H.; Hong, Z.; Zhou, H.; Yang, Y. Under the spotlight: The organic−inorganic hybrid halide perovskite for optoelectronic applications. *Nano Today* **2015**, *10*, 355−396.

(6) Ahn, N.; Son, D.-Y.; Jang, I.-H.; Kang, S. M.; Choi, M.; Park, N.-G. Highly Reproducible Perovskite Solar Cells with Average Efficiency of 18.3% and Best Efficiency of 19.7% Fabricated via Lewis Base Adduct of Lead(II) Iodide. *J. Am. Chem. Soc.* **2015**, *137*, 8696−8699. PMID: 26125203.
(7) Green, M. A.; Dunlop, E. D.; Yoshita, M.; Kopidakis, N.; Bothe, K.; Siefer, G.; Hinken, D.; Rauer, M.; Hohl-Ebinger, J.; Hao, X. Solar cell efficiency tables (Version 64). *Progress in Photovoltaics: Research and Applications* **2024**, *32*, 425−441.
(8) Eames, C.; Frost, J. M.; Barnes, P. R. F.; O'Regan, B. C.; Walsh, A.; Islam, M. S. Ionic transport in hybrid lead iodide perovskite solar cells. *Nat. Commun.* **2015**, *6*, 7497.
(9) Xing, J.; Wang, Q.; Dong, Q.; Yuan, Y.; Fang, Y.; Huang, J. Ultrafast ion migration in hybrid perovskite polycrystalline thin films under light and suppression in single crystals. *Phys. Chem. Chem. Phys.* **2016**, *18*, 30484−30490.
(10) Domanski, K.; et al. Migration of cations induces reversible performance losses over day/night cycling in perovskite solar cells. *Energy Environ. Sci.* **2017**, *10*, 604−613.
(11) Lin, L.; Yang, L.; Du, G.; Li, X.; Li, Y.-n.; Deng, J.; Wei, K.; Zhang, J. Light Soaking Effects in Perovskite Solar Cells: Mechanism, Impacts, and Elimination. *ACS Applied Energy Materials* **2023**, *6*, 10303−10318.
(12) Bennett, L. J.; Riquelme, A. J.; Courtier, N. E.; Anta, J. A.; Richardson, G. A new ideality factor for perovskite solar cells and an analytical theory for their impedance spectroscopy response. *arXiv* **2021**.
(13) Mahapatra, A.; Parikh, N.; Kumar, P.; Kumar, M.; Prochowicz, D.; Kalam, A.; Tavakoli, M. M.; Yadav, P. Changes in the Electrical Characteristics of Perovskite Solar Cells with Aging Time. *Molecules* **2020**, *25*, 2299.
(14) Riquelme, A.; Bennett, L. J.; Courtier, N. E.; Wolf, M. J.; Contreras-Bernal, L.; Walker, A. B.; Richardson, G.; Anta, J. A. Identification of recombination losses and charge collection efficiency in a perovskite solar cell by comparing impedance response to a drift-diffusion model. *Nanoscale* **2020**, *12*, 17385−17398.
(15) Pitarch, Á.; Garcia-Belmonte, G.; Mora-Seró, I.; Bisquert, J. Electrochemical impedance spectra for the complete equivalent circuit of diffusion and reaction under steady-state recombination current. *Phys. Chem. Chem. Phys.* **2004**, *6*, 2983−2988.
(16) Lai, W. Fourier Analysis of Complex Impedance (amplitude and phase) in Nonlinear systems: a Case Study of Diodes. *Electrochim. Acta* **2010**, *55*, 5511−5518.
(17) Larsen, A.; Dahal, E.; Paluba, J.; Cianciulli, K.; Isenhart, B.; Arnold, M.; Du, B.; Jiang, Y.; White, M. S. Nonlinear Impedance Spectroscopy of Organic MIS Capacitors and Planar Heterojunction Diodes. *Org. Electron.* **2018**, *62*, 660−666.
(18) Wilson, J.; Schwartz, D.; Adler, S. Nonlinear electrochemical impedance spectroscopy for solid oxide fuel cell cathode materials. *Electrochim. Acta* **2006**, *51*, 1389−1402. Electrochemical Impedance Spectroscopy
(19) Liebhart, B.; Satzke, M.; Komsiyska, L.; Endisch, C. Application of nonlinear impedance spectroscopy for the diagnosis of lithium-ion battery cells under various operating conditions. *J. Power Sources* **2020**, *480*, No. 228673.
(20) Thiébaut, E.; Pesty, F.; Goupil, C.; Guegan, G.; Lecoeur, P. Non-linear impedance spectroscopy for complete thermoelectric characterization: Beyond the zT estimation. *J. Appl. Phys.* **2018**, *124*, 235106.
(21) Fleig, J.; Jamnik, J.; Maier, J.; Ludvig, J. Inductive Loops in Impedance Spectroscopy Caused by Electrical Shielding. *J. Electrochem. Soc.* **1996**, *143*, 3636.
(22) Butcher, K.; Tansley, T.; Alexiev, D. An instrumental solution to the phenomenon of negative capacitances in semiconductors. *Solid-State Electron.* **1996**, *39*, 333−336.
(23) Wu, X.; Yang, E. S.; Evans, H. L. Negative capacitance at metal-semiconductor interfaces. *J. Appl. Phys.* **1990**, *68*, 2845−2848.
(24) Werner, J. H. Comment on "Negative capacitance at metal-semiconductor interfaces". *J. Appl. Phys.* **1991**, *70*, 1087−1088. [J. Appl. Phys. 68, 2845 (1990)].
(25) Ebadi, F.; Aryanpour, M.; Mohammadpour, R.; Taghavinia, N. Coupled ionic-electronic equivalent circuit to describe asymmetric rise and decay of photovoltage profile in perovskite solar cells. *Sci. Rep.* **2019**, *9*, 11962.
(26) Zhao, Y.-C.; Zhou, W.-K.; Zhou, X.; Liu, K.-H.; Yu, D.-P.; Zhao, Q. Quantification of light-enhanced ionic transport in lead iodide perovskite thin films and its solar cell applications. *Light: Science & Applications* **2017**, *6*, No. e16243.
(27) Urbaniak, A.; Czudek, A.; Dagar, J.; Unger, E. Capacitance spectroscopy of thin-film formamidinium lead iodide based perovskite solar cells. *Sol. Energy Mater. Sol. Cells* **2022**, *238*, No. 111618.
(28) Zuo, L.; Li, Z.; Chen, H. Ion Migration and Accumulation in Halide Perovskite Solar Cells. *Chin. J. Chem.* **2023**, *41*, 861−876.
(29) Pockett, A.; Eperon, G. E.; Sakai, N.; Snaith, H. J.; Peter, L. M.; Cameron, P. J. Microseconds, milliseconds and seconds: deconvoluting the dynamic behaviour of planar perovskite solar cells. *Phys. Chem. Chem. Phys.* **2017**, *19*, 5959−5970.
(30) Rybin, N.; Ghosh, D.; Tisdale, J.; Shrestha, S.; Yoho, M.; Vo, D.; Even, J.; Katan, C.; Nie, W.; Neukirch, A. J.; Tretiak, S. Effects of Chlorine Mixing on Optoelectronics, Ion Migration, and Gamma-Ray Detection in Bromide Perovskites. *Chem. Mater.* **2020**, *32*, 1854−1863.
(31) Futscher, M. H.; Gangishetty, M. K.; Congreve, D. N.; Ehrler, B. Manganese Doping Stabilizes Perovskite Light-Emitting Diodes by Reducing Ion Migration. *ACS Applied Electronic Materials* **2020**, *2*, 1522−1528.
(32) Pering, S. R.; Cameron, P. J. The effect of multiple ion substitutions on halide ion migration in perovskite solar cells. *Mater. Adv.* **2022**, *3*, 7918−7924.
(33) Deng, X.; Wen, X.; Zheng, J.; Young, T.; Lau, C. F. J.; Kim, J.; Green, M.; Huang, S.; Ho-Baillie, A. Dynamic study of the light soaking effect on perovskite solar cells by in-situ photoluminescence microscopy. *Nano Energy* **2018**, *46*, 356−364.

https://doi.org/10.1021/acsaem.5c00672
ACS Appl. Energy Mater. XXXX, XXX, XXX−XXX